Available online at www.sciencedirect.com
SCIENCE DIRECT®
Synthetic Metals 149 (2005) 63–72
SYNTHETIC METALS
www.elsevier.com/locate/synmet

Chlorine precursor route to poly(2-phenoxy *p*-phenylene vinylene): synthesis and characterization

James N. Wilking[1], Bing Hsieh[2], Georgia A. Arbuckle-Keil*

Department of Chemistry, Rutgers University, 315 Penn Street, Camden, NJ 08102, USA

Received 6 October 2004; received in revised form 5 November 2004; accepted 8 November 2004
Available online 8 January 2005

Abstract

A new PPV derivative, poly(2-phenoxy *p*-phenylene vinylene)(PO-PPV), has been synthesized via the chlorine precursor route (CPR). PO-PPV and its chlorine precursor polymer were fully characterized by thermal (TGA and DSC), mechanical and spectroscopic (UV–vis, PL and IR) methods. The results indicate that the precursor polmer and the yellow-green light-emitting PO-PPV have excellent stability and mechanical properties. The easily processible precursor is stable at room temperature and therefore has a better shelf-life than PPV synthesized via the sulfonium precursor route. Thermal conversion provides high quality films, relatively free of oxidative defects.

Keywords: PO-PPV; Poly(2-phenoxy *p*-phenylene vinylene); PPV derivative; Chlorine precursor route; Photoluminescence; Thermal analysis; FT-IR

1. Introduction

Conjugated conducting polymers are distinguished from other electroactive polymers by their intrinsic semiconductivity, independent of solvation or a conducting filler, and inherent to their extended conjugation along the polymer backbone. These polymers are unique, in that near-metallic conductivity can be induced by doping with oxidative or reductive agents. The unique properties of conducting polymers are directly related to their delocalized electronic structure. The first twenty years of research on conducting polymers were focused on achieving maximum conductivities through doping. This focus shifted in 1990 when the discovery of electroluminescence in a conducting polymer was reported in poly(*p*-phenylene vinylene) (PPV) [1]. Subsequent research revealed that the attachment of various substituents to the conjugated backbone altered the electronic structure of the polymer and therefore altered the emission wavelength. This provided the ability to tune the light-emitting properties of the polymer by changing the molecular structure. Such an approach has led to the synthesis of numerous PPV derivatives, which have been investigated extensively for their potential use in optoelectronic devices, [2] particularly organic light emitting diodes (OLED's).

An OLED is fabricated by sandwiching the polymer between a high work function and low work function electrode [3]. A potential is then applied across the polymer, resulting in the injection of electrons from the low work function cathode into the LUMO, and the injection of positive holes from the high work function anode into the HOMO. The opposite charges combine within the polymer to form *excitons* that radiatively decay, emitting a photon. PPV and PPV derivatives are among the most promising optoelectronic materials, though problems with processing, stability and quantum efficiency must be overcome.

* Corresponding author.
E-mail address: arbuckle@camden.rutgers.edu (G.A. Arbuckle-Keil).
[1] Department of Chemistry and Biochemistry, Box 951569, UCLA, Los Angeles, CA 90095-1569, USA.
[2] Nukote International Inc., 1227 Ridgeway Avenue, Rochester, NY 14615, USA.

0379-6779/$ – see front matter © 2004 Elsevier B.V. All rights reserved.
doi:10.1016/j.synthmet.2004.11.004

Due to their insolubility, PPV's are commonly synthesized via precursor routes [4]. A variety of routes have been developed, involving a processible precursor polymer which can be thermally converted to the conjugated PPV product after processing [5]. The chlorine precursor route (CPR), first developed by Swatos and Gordon [6] and later modified by Hsieh, [7,8] has proven useful in the synthesis of phenylated PPV's. A number of PPV's with bulky substituents have been reportedly synthesized via the CPR [9]. The CPR yields a high molecular weight precursor polymer, generally soluble in organic solvents. Thermal conversion under a reducing atmosphere is not necessary to obtain PPV's relatively free of oxidative defects, making this route ideal for optoelectronic applications [6]. Oxidative defects quench luminescence and result in lower quantum efficiencies. We report here the complete synthesis of a new PPV derivative, poly(2-phenoxy *p*-phenylene vinylene)(PO-PPV) via the chlorine precursor route. We have previously reported some of the optoelectronic properties of this polymer that were investigated using dynamic infrared spectroscopy; the ring stretches associated with the backbone phenylene were distinguished from the ring stretches of the phenoxy substituent [10]. Cohesive free-standing films of PO-PPV can be prepared. The thermal (TGA and DSC), mechanical and optical (UV–vis, photoluminescence, FT-IR) properties of PO-PPV are presented here.

2. Experimental

The synthesis of the monomer, 2-phenoxy-1,4-bis(chloromethyl)benzene (2), was performed in two steps, as shown in Fig. 1. The first step involved the reduction of 2-phenoxyterephthalic acid to yield 2-phenoxy-1,4-bis(hydroxymethyl)benzene (1); in the second step, (1) was treated with thionyl chloride to produce the monomer as detailed below (2). The monomer was polymerized to yield the precursor polymer (3) (Fig. 1).

2.1. Synthesis of 2-phenoxy-1,4-bis(hydroxymethyl)benzene (1)

2-Phenoxyterephthalic acid [11] (15.6 g, 0.06 mol) was placed in a 1 l three-neck round bottom flask equipped with a condenser, mechanical stirrer, an addition funnel and a nitrogen inlet. THF (180 ml) was added to the acid to give a solution. 1.0 M $LiAlH_4$ in THF (270 ml) was transferred into the addition funnel and added at a moderate rate to the solution. The resulting mixture was stirred for 20 h and then quenched by drop wise addition of water (25 ml). This was followed by addition of 16% NaOH (60 ml). The white precipitate was removed by suction filtration and washed with chloroform (200 ml). The filtrate was extracted with ether (3 × 150 ml). The organic phase was allowed to stand overnight in a separatory funnel to ensure complete water separation, poured through a folded filter paper into a 1 l round bottom flask and concentrated to give a white solid. This was air dried to give 12.0 g (87%) of crude (1) as an off-white powder. This was used without further purification in the next step because it showed the expected clean ^{1}H NMR ($CDCl_3$): δ 7.42 (d, 1H), 7.35 (t, 2H), 7.10 (m, 2H), 6.96 (d, 2H), 6.86 (s, 1H), 4.72 (s, 2H). 4.60 (s, 2H).

2.2. Synthesis of 2-phenoxy-1,4-bis(chloromethyl)benzene (2)

To a mixture of crude (1) (9.2 g), methylene chloride (100 ml), and $SOCl_2$ (12.0 g), three drops of pyridine was added. The resulting mixture was refluxed overnight and then concentrated in vacuo to give a light yellow oil. This was vacuum distilled to give (2) as a light yellow oil (140–141 °C/0.1 mmHg): ^{1}H NMR ($CDCl_3$): δ 7.44 (d, 1H), 7.34 (t, 2H), 7.12 (t, 2H), 7.00 (d, 2H), 6.86 (s, 1H), 4.66

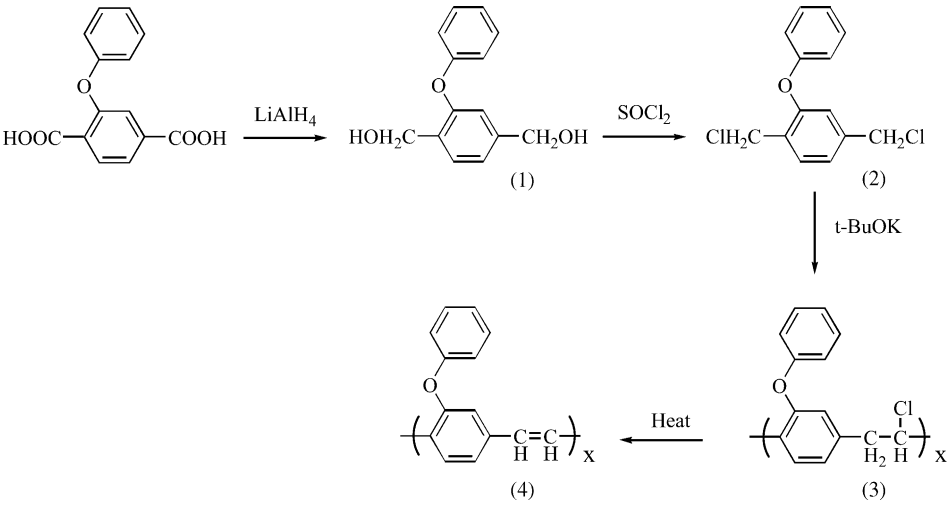

Fig. 1. The synthesis of poly(2-phenoxy *p*-phenylene vinylene).

(s, 2H), 4.45 (s, 2H); Anal. Calcd. for $C_{14}H_{12}Cl_2O$: C, 62.92; H, 4.49; Cl, 26.59. Found: C, 62.82; H, 4.64; Cl, 26.62.

2.3. Synthesis of 2-phenoxy p-phenylenevinylene precursor polymer (3)

Into a 500 ml three neck round bottom flask equipped with a magnetic stirrer, an addition funnel and a nitrogen inlet was added (2) (4.0 g, 0.015 mol) and THF (150 ml). Into the addition funnel was added 1.0 M *t*-BuOK/THF (15 ml, 0.015 mol). This was added rapidly into the (2)/THF solution. Polymerization took place quickly with the formation of small amount of light orange gel and continued for 2 h. The gel was removed with a spatula and the reaction mixture was poured gradually into stirring methanol (600 ml). The precipitated fibril material was collected by suction filtration and washed with methanol and air dried to give 1.9 g (55%) of (3) as pale yellow fibers. Elemental analysis showed C, 74.10; H, 5.20; Cl, 12.95. This is close to that for a material with 18% conversion: C, 75.02; H, 4.83; Cl, 13.00. The GPC M_w, M_n and M_w/M_n were 660,000, 134,000 and 4.9, respectively.

2.4. Preparation of free-standing polymer films

Free-standing films of the PO-PPV precursor and PO-PPV were obtained in varying thicknesses by the following method. PO-PPV precursor films were cast on a Teflon substrate from a 0.35 w/v % chloroform solution. Thermal conversion of these films under an inert atmosphere at 280 °C for 1 h yielded high-quality free-standing PO-PPV films. Free-standing films were used in the following analyses: X-ray diffraction, differential scanning calorimetry (DSC), photoluminescent (PL) spectroscopy, dynamic mechanical analysis (DMA) and infrared (IR) spectroscopy. Additional sample preparation unique to each technique is mentioned when relevant.

2.5. Instrumentation

2.5.1. Thermogravimetric analysis (TGA)

Thermogravimetric analysis of the PO-PPV precursor was performed using a TGA 2050 (TA Instruments, New Castle, DE). The samples were heated from ambient temperature, through complete thermal conversion, to 325 °C. Heating rates of 2, 3, 5, 7, and 9 °C/min were used. The PO-PPV precursor polymer was compacted into pellet form. In order to minimize thermal lag, samples were <5 mg in size. Kinetic studies on the experimental data were performed using a TGA kinetics program (Thermal Specialty Library, Version 1.00F, TA Instruments).

Evolved gases were analyzed by coupling the TGA, via a heated transfer line, to a FTS 6000 FT-IR spectrometer (Digilab USA, Randolph, MA). The spectrometer was equipped with a gas cell fitted with ZnSe windows and a deuterated triglycine sulfate (DTGS) detector with a low-energy spectral limit of 400 cm^{-1}.

2.5.2. Differential scanning calorimetry (DSC)

Differential scanning calorimetry was performed on PO-PPV and PO-PPV precursor pellets using a DSC 2920 (TA Instruments, New Castle, DE). Thermal analyses were performed under an inert atmosphere of nitrogen. In order to minimize thermal lag, samples were <5 mg in size. Polymer samples were hermetically sealed in aluminum pans and heated at a rate of 10 °C/min from ambient temperature to 300 °C.

2.5.3. Dynamic mechanical analysis

The mechanical properties of PO-PPV and the precursor polymer were analyzed with a dynamic mechanical analyzer (DMA) 2980, (TA Instruments, New Castle, DE), equipped with a film tension clamp. Film samples were approximately 12 mm × 7 mm × 0.02 mm in size. A sample modulation frequency of 16 Hz, amplitude of 25 μm, heating rate of 1 °C/min, and temperature range of 25–140 °C were used.

2.5.4. X-ray diffraction

The crystallinity of PO-PPV films were measured using a Rigaku D/M-2200T X-Ray Diffractometer. An operating power of 40 k/40 mA, step size of 0.02 in 2θ and a scan rate of 1.7°/min were used.

2.5.5. Ultraviolet–visible spectroscopy (UV–vis)

Absorption spectra of thin PO-PPV and PO-PPV precursor films were obtained in the ultraviolet–visible region (200–800 nm). Optically thin films of the PO-PPV precursor were cast from a 0.35 w/v% chloroform solution onto 330 cm thick circular (1 in. diameter) quartz plates. Films were thermally converted to PO-PPV and final thicknesses were approximately 5–10 μm. Data collection was performed on the films before and after thermal conversion using a Varian-Cary 5E UV–vis–NIR spectrophotometer. A spectral resolution of 1 nm was achieved at a scan rate of 100 nm/min.

2.5.6. Photoluminescent spectroscopy (PL)

The luminescent properties of PO-PPV film were recorded using a fluorescence spectrophotometer (Eclipse Series, Varian-Cary). Film thickness was approximately 15 μm. The sample was irradiated at a 45° angle of incidence. An excitation wavelength of ∼434 nm was used, and the region 460–700 nm was scanned for emission at a rate of 600 nm/min. Both the excitation and emission slit widths were 5 nm.

2.5.7. Fourier transform infrared spectroscopy (FT-IR)

2.5.7.1. Transmission infrared. Measurements were performed on free-standing films of PO-PPV and the PO-PPV precursor. A Bio-Rad FTS 6000 FT-IR spectrometer (Digilab USA, Randolph, MA) in rapid scan mode was used to collect

data. A spectral resolution of 4 cm^{-1} and a deuterated triglycine sulfate (DTGS) detector with a low-energy spectral limit of 400 cm^{-1} was used for all infrared studies.

2.5.7.2. In situ transmission infrared. Studies of the thermal conversion from PO-PPV precursor to PO-PPV (Fig. 1) were performed in the FTS 6000 spectrometer using a heated cell (HTC 100, Harrick Scientific, Ossining, NY). The KBr cell windows were water-cooled using a re-circulating chiller (1013S, Fisher Scientific). The temperature of the cell was controlled with an automatic temperature feedback controller (AT-30D, Harrick Scientific). Films of the precursor polymer, approximately 10–20 μm in thickness, were heated in the in situ cell at a rate of 5 °C/min from ambient temperature to 300 °C while spectral changes were monitored.

2.6. Density functional theory (DFT) calculations

The infrared spectra of both PO-PPV and its precursor polymer were calculated by Dr. Paul Maslen, Rutgers University. In both cases a six-monomer ring was used to model an extended polymer chain. Structure optimization and frequency calculations were performed using Q-Chem 2.0, [12] an electronic structure program package. A Gauss View graphics package was used to visualize the results. The Becke's three-parameter exchange functional [13] was used, in combination with the Lee–Yang–Parr correlation functional [14] (B3LYP) and 3–21G basis set, for both calculations.

3. Results and discussion

3.1. Synthesis

The synthesis of the monomer, 2-phenoxy-1,4-bis(chloromethyl)benzene (2), was performed in two steps, as shown in Fig. 1. The reduction of 2-phenoxyterephthalic acid with lithium aluminum hydride to yield (1) was followed by treatment with thionyl chloride to produce (2). Polymerization was induced by treatment with 1.0 equiv. of potassium *tert*-butoxide to yield the phenoxy precursor polymer (3). The precursor polymer was found to have a M_w of 660,000, a M_n of 134,000 and a molecular weight distribution (M_w/M_n) of 4.9. Elemental analysis indicated 18% conversion based on the chlorine content. The chlorine precursor polymer was readily soluble in chloroform.

3.2. Thermogravimetric analysis

Thermogravimetric analysis (TGA) was used to monitor the weight loss during thermal conversion of the PO-PPV precursor to PO-PPV under an inert atmosphere of nitrogen gas. Conversion occurs as a β-dehydrohalogenation involving the loss of HCl (Fig. 1). As shown by the thermogravimetric curve in Fig. 2, the PO-PPV precursor undergoes approximately 13% weight loss via a single step. This corresponds to the loss of HCl from the PO-PPV precursor (18% converted as shown by elemental analysis), which would theoretically result in a weight loss of 13.3%. A theoretical weight loss of 15.8% would be expected for a pure precursor. Thermal conversion is complete at approximately 300 °C. PO-PPV shows thermal stability up to 325 °C. The analysis of evolved gases and the Gram–Schmidt chromatogram included in Fig. 2 will be discussed (vide infra).

The stability of the PO-PPV precursor is of interest, as a number of PPV and PPV derivative precursors are unstable and must be stored at sub-ambient temperatures to prevent conversion. The particularly unstable sulfonium PPV precursor has a half-life of only a few days at room temperature. [15] The xanthate PPV precursor is stable, relative to the sulfonium precursor, but experiences long-term instability. Thermogravimetric data can be used to approximate important kinetic parameters such as activation energy and precursor half-life. The details of this thermogravimetric kinetics approach, based on the Arrhenius rate equation, have been discussed elsewhere. [16,17] The calculated activation energies and 60 min half-life temperatures at various points

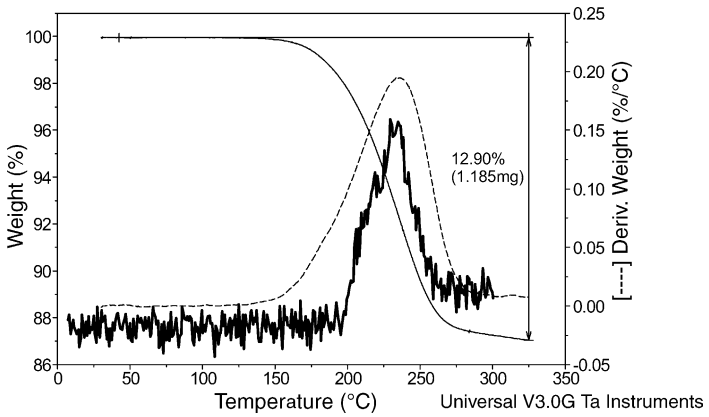

Fig. 2. TGA curve (smooth solid line), the DTGA (weight change with respect to temperature) (dashed line) and Gram–Schmidt chromatogram of evolved HCl (noisy bold line) during heating of PO-PPV precursor polymer from room temperature to ~300 C.

Table 1
Kinetic values for the PO-PPV precursor

Conversion (%)	Activation energy (kJ/mol)	60 min half-life temperature (°C)
1	112.2	164.8
2	117.4	165.4
5	111.4	167.8
10	115.0	169.6
15	117.8	171.6
20	119.9	173.4
25	121.5	175.0

of thermal conversion are listed in Table 1[18]. Although small conversion levels such as 1% and 2% often involve some initial volatilization of solvent or moisture, as shown in Table 1, the values are fairly consistent across the range of conversion levels. This indicates that the same mechanism of elimination is occurring throughout the thermal elimination. The kinetic parameters at a conversion level of 5% can be chosen as representative of the PO-PPV precursor. Extrapolation of the 60 min half-life temperature at 5% provides a room temperature half-life of hundreds of years, indicating long-term stability and an extended shelf-life.

3.3. Differential scanning calorimetry

Differential scanning calorimetry (DSC) was performed on both the PO-PPV precursor and PO-PPV. The T_g is observed experimentally with DSC as an endothermic step. The DSC plots of PO-PPV and the PO-PPV precursor are not shown. The DSC results indicate that the PO-PPV and its precursor exhibit T_g's at 123 °C and 59 °C, respectively. The T_g of PO-PPV is significantly lower than that reported for PPV: (∼370 °C) [19] or (∼220 °C) [20] depending on synthesis and thermal conversion conditions. In contrast, the T_g for MEH-PPV is much lower, ∼65 °C [21]. The glass transition temperatures for PO-PPV precursor and PO-PPV have been supported by dynamic mechanical analysis [10]. The PO-PPV precursor also exhibits a strong endotherm at 210 °C, corresponding to the temperature of maximum weight loss observed by TGA. An enthalpy change such as this is expected as dehydrochlorination is occurring during thermal conversion. No endotherm is present in the DSC plot of PO-PPV indicating that thermal conversion is complete. It should also be noted that no melting transition is observed in PO-PPV before thermal decomposition (∼325 °C).

3.4. Dynamic mechanical analysis

The mechanical properties of PO-PPV and the PO-PPV precursor have been reported in detail elsewhere [10]. Dynamic mechanical studies have shown that PO-PPV exhibits a higher storage modulus, lower loss modulus and smaller tan δ at room temperature than the PO-PPV precursor. The storage modulus of PO-PPV at room temperature (∼2.4 GPa) is comparable to that reported for polyaniline (∼2.5 GPa) [22] and higher than that of PPV (∼1.8 GPa) [23] and polypyrrole (∼0.5 GPa) [24]. The tan δ values for PO-PPV and the PO-PPV precursor at room temperature are 0.02 and 0.06 radians, respectively. As mentioned previously, the glass transition values determined by DSC are supported by peaks in tan δ at 57 °C and 128 °C, respectively. In the case of both PO-PPV and the PO-PPV precursor, the glass transition is accompanied by a complete loss of storage modulus, indicating a totally amorphous polymer. Crystalline regions within a non-amorphous polymer prevent the complete loss of storage modulus.

3.5. X-ray diffraction

X-ray analysis revealed that PO-PPV was completely amorphous. No diffraction peaks were observed, even after conversion at 280 °C for 2 h. Amorphous PPV, achieved by the introduction of *cis*-linkages, has been shown to have more favorable electroluminescence than crystalline PPV [25]. The presence/absence of *cis*-linkages in PO-PPV could not be confirmed by FT-IR (vide infra). Disruption of crystalline packing is likely caused by the pendant phenoxy group.

3.6. Ultraviolet–visible spectroscopy

The UV–vis spectra for PO-PPV and the PO-PPV precursor (thin lines) are shown in Fig. 3. This region of the electromagnetic spectrum is energetically sufficient to promote electronic transitions from the valence to conduction bands, resulting in a broad π–π^* transition absorption in the UV–vis spectrum for the conjugated polymer, PO-PPV. This prominent absorption is observed in PO-PPV (Fig. 3, thin line) with a $\lambda_{max,\ abs}$ at 434 nm. The absence of any vibronic structure indicates an amorphous polymer and supports the X-ray data. An experimental band gap of 2.40 eV can be calculated from the low energy absorption edge of the π–π^* transition peak. This value is approximately the same as that reported

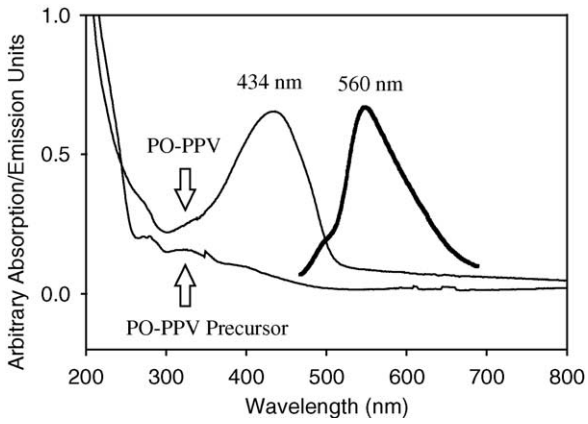

Fig. 3. UV–vis spectra of PO-PPV precursor, PO-PPV (thin lines) and photoluminescence spectrum (thick line) of PO-PPV excited at 434 nm.

for PPV synthesized via the Wessling precursor route [26]. While the band gap of PO-PPV would be expected to shift relative to PPV, due to the electron-donating phenoxy substituent, additional factors such as conjugation length and molecular weight also influence the resulting band gap.

3.7. Photoluminescent spectroscopy

The photoluminescent spectra of PO-PPV is shown in Fig. 3 (thick line). The π–π^* $\lambda_{max,\ abs}$ at 434 nm in the UV–vis spectrum was chosen as the excitation wavelength. PO-PPV exhibits a strong $\lambda_{max,\ em}$ at 560 nm and is therefore, a yellow-green light-emitting PPV. While this wavelength of emission is not unique among PPV's, the processibility of the PO-PPV precursor and low defect nature of PO-PPV may prove useful in opto-electronic applications. X-ray analysis, UV–vis spectra and dynamic mechanical analysis have indicated that PO-PPV is an amorphous polymer. This disorder is expected to result in a high PL quantum efficiency, as it has been shown that close-packing of conjugated polymers results in self-quenching [27].

3.8. Fourier transform infrared spectroscopy (FT-IR)

3.8.1. Evolved gas analysis

FT-IR analysis of the evolved gases during heating (TGA) verifies that HCl is lost from the precursor during thermal elimination. The characteristic vibrational–rotational spectrum of HCl shown in Fig. 4 is prominent throughout the period of weight loss. No other characteristic infrared vibrational modes are observed. This is expected based on the thermal elimination reaction shown in Fig. 1. A Gram–Schmidt chromatogram for the HCl vibrational–rotational infrared feature of Fig. 4 is displayed as the bold solid line in Fig. 2. The chromatogram plots the intensity of this particular infrared feature with respect to temperature. It can be seen that the maximum of HCl elimination (chromatogram) corresponds with the point of maximum weight loss (DTGA).

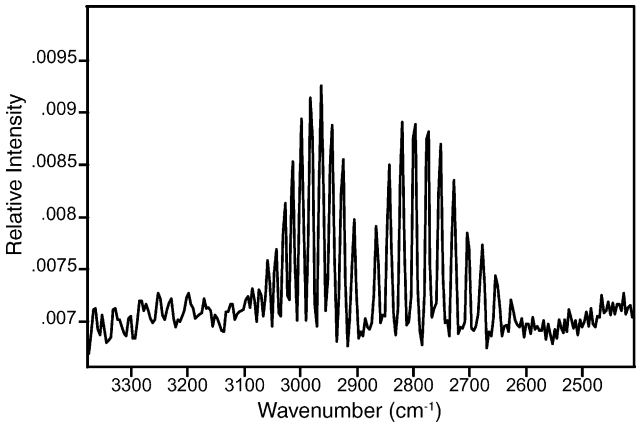

Fig. 4. Vibrational–rotational spectrum of HCl eliminated from the PO-PPV precursor during thermal conversion.

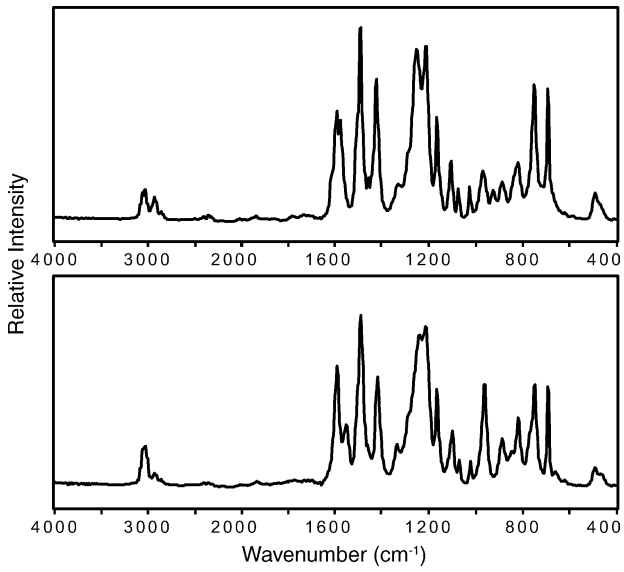

Fig. 5. The infrared absorbance spectra of PO-PPV precursor (upper) and the PO-PPV (lower) in the 4000–400 cm^{-1} region.

3.8.2. Identification of characteristic infrared vibrational modes

The infrared absorbance spectra of both PO-PPV and the PO-PPV precursor in the 4000–400 cm^{-1} region are shown in Fig. 5. The 2000–400 cm^{-1} region of each plot has been expanded by a factor of two relative to the 4000–2000 cm^{-1} region. The infrared vibrational modes of PO-PPV are discussed and identified here. Assignments are made based on the following: previously identified vibrational modes of PPV, [28] characteristic group frequencies in the literature, [29] density functional theory IR spectra calculations, spectral changes observed during in situ analysis of the thermal elimination reaction and dynamic infrared studies. [10] The assignments for PO-PPV, made in this study, are listed in Table 2 along with the vibrational modes of PPV obtained from the literature. [28] The band assignments for PPV have been well established and have proven beneficial in the identification of the vibrational spectra of PO-PPV.

Density functional theory (DFT) infrared spectral calculations for both PO-PPV and its precursor were performed to support the assignments of infrared normal modes. A list of characteristic vibrational frequencies with relative intensities was generated for each polymer. The calculated frequencies provide strong support in the identification of the infrared vibrational bands. All theoretical frequencies were higher in energy than their corresponding experimental bands, and a shift of approximately $-50\ cm^{-1}$ was necessary to obtain an acceptable match. The theoretical (histogram) and experimental spectra for PO-PPV in the 1700–500 cm^{-1} regions are overlaid in Fig. 6. The theoretical and experimental spectra for the PO-PPV precursor (not shown) exhibit a similar match. Factors which limited the accuracy of these calculations include: the neglect of anharmonicity, approximations inherent in the basis set and B3LYP functional, the use of a

Table 2
Comparison of experimental infrared vibrational frequencies and assignments for PPV [28] and PO-PPV

Assignment	PPV (cm^{-1})	PO-PPV (cm^{-1})
Aromatic C─H str.	3076(w), 3047(w)	–
Trans-vinylene C─H str. and/or aromatic C─H str.	–	3067(w)
Trans-vinylene C─H str.	3024(s)	3030(w)
Aliphatic C─H str.	2950(w), 2920(w), 2852(w)	2956(w), 2928(w), 2860(w)
C═O str.	1696(w)	–
C–C ring str. ('quadrant')	1594(w)	–
C–C ring str. ('semi-circle')	1519(vs), 1424(m)	–
C–C ring str. (origin unknown)	1336(m)	1590(s), 1549(m), 1339(m)
C–C ring str. (backbone)	–	1504(m)*, 1421(s)*
C–C ring str. (backbone and phenoxy)	–	1488(vs)*
C–O–C str.	–	1235(vs)*, 1210(vs)*, 1162(s)
p-phenylene C─H in-plane bend	1267(w), 1176(w), 1108(m), 1013(w)	–
Vinylene C─H in-plane bend	1210(w)	–
C─H in-plane bend	–	1098(m), 1069(w), 1021(w)
Trans-vinylene C─H out-of-plane bend	965(vs)	958(s)
p-phenylene C─H out-of-plane bend	837(vs), 556(s)	–
C─H out-of-plane bend	–	885(m), 843(m), 816(m)
Origin unknown	784(s)	–
Phenoxy C─H out-of-plane bend	–	750(s)*, 690(s)*

* Assignments supported by dynamic infrared spectroscopy.

six-monomer ring to simulate an extended polymer and assumptions regarding the molecular geometry and polymer tacticity.

In situ infrared spectroscopy is used to follow spectral changes which occur during thermal conversion. The relatively few frequency shifts/intensity changes which were observed during the conversion of the PO-PPV precursor to PO-PPV are highlighted in Fig. 7a–d. The arrows indicate the direction of relative intensity increase or decrease on conversion from PO-PPV precursor to PO-PPV. These changes provide additional support in the identification of the vibrational modes and will be discussed below.

Dynamic infrared spectroscopy studies have been performed on PO-PPV and the PO-PPV precursor and reported elsewhere. [10] Assignments which are supported by these dynamic studies are discussed briefly and are indicated in Table 2. These assignments have been made based on a spectroscopic response to an applied perturbation.

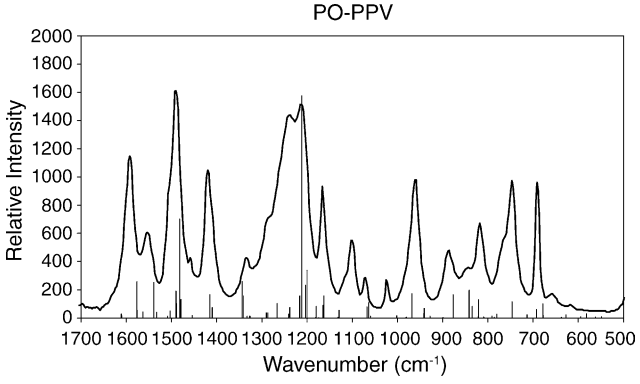

Fig. 6. The experimental and theoretical (histogram) infrared spectra of PO-PPV in the 1700–500 cm^{-1} region.

3.8.3. *Hydrocarbon region 3200–2800 cm^{-1}*

Three types of C–H stretches occur in the hydrocarbon region (3200–2800 cm^{-1}): aromatic, vinylene, and aliphatic. The infrared absorbance spectra of PO-PPV and PPV in this region are displayed in Fig. 8. The following C–H stretches occur in this region in decreasing energy: aromatic, vinylene and aliphatic. Overlaid in situ spectra of the PO-PPV precursor in this region at various points of thermal conversion to PO-PPV are shown in Fig. 7a. It is apparent that peaks at 3067 and 3030 cm^{-1} increase significantly in intensity, while the intensities of vibrations at 2956 and 2928 cm^{-1} decrease modestly. A strong peak at 3024 cm^{-1} in the PPV spectra has been identified as the *trans*-vinylene C–H stretch and this mode is likely responsible for the peak at 3030 cm^{-1} in the PO-PPV precursor (Fig. 8). It may seem unusual that the increase in intensity is less than expected (Fig. 7a). This can be explained by the fact that the precursor polymer exhibits 18% conversion before thermal conversion to PO-PPV. Aromatic C–H stretches are very weak in the spectrum of PPV (Fig. 8). The presence of the aromatic phenoxy substituent in PO-PPV is expected to complicate the aromatic C–H region with respect to the spectrum of PPV. The peak at 3067 cm^{-1}, which is not present in PPV, is likely associated with aromatic C–H stretching associated with the phenoxy substituent. However, it undergoes a strong increase in intensity along with the *trans*-vinylene C–H stretch at 3030 cm^{-1} (Fig. 7a). Its association with delocalized vinylene and phenoxy C–H stretching is supported by the DFT results. While calculated vibrational frequencies in the hydrocarbon region (not shown) of PO-PPV do not provide an exact match with the experimental spectra, they do support all assignments in this region. Two vibrations at 2956 and 2928 cm^{-1} decrease in intensity during thermal conversion (Fig. 7a), while the peak at 2860 cm^{-1} remains relatively

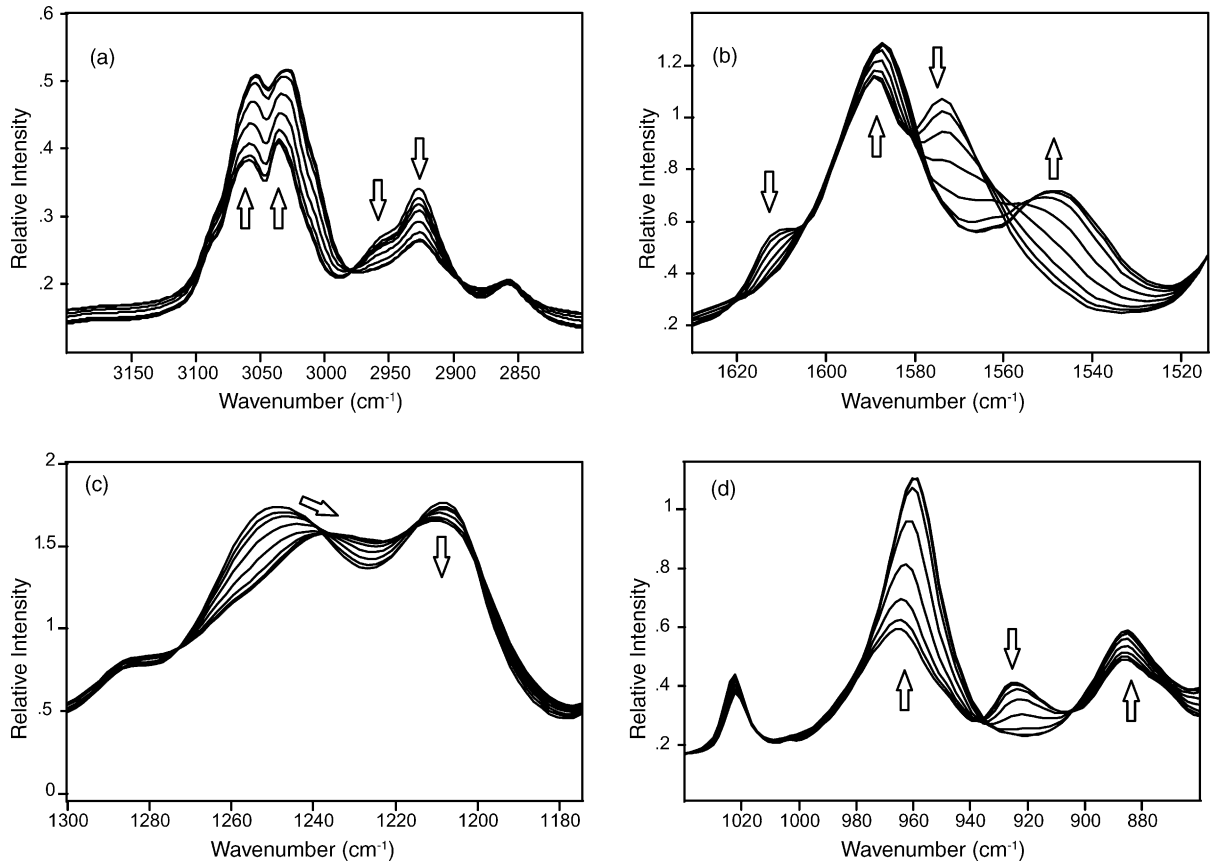

Fig. 7. In situ spectra of the PO-PPV precursor undergoing thermal conversion to PO-PPV in the regions: (a) 3200–2800 cm^{-1}, (b) 1625–1510 cm^{-1}, (c) 1300–1175 cm^{-1}, (d) 1040–860 cm^{-1}.

unchanged. These vibrations can be confidently labeled as aliphatic C–H stretches. Theoretically, these stretches would be absent in a fully conjugated polymer. They are also present to a small extent in PPV, where they have been labeled as aliphatic C–H stretches (Table 2) and are most likely due to polymer endgroups.

3.8.4. *Fingerprint region: 1700–600 cm^{-1}*

The infrared absorbance spectra of PO-PPV and PPV over the entire fingerprint region (1700–600 cm^{-1}) are overlaid in Fig. 9. Oxidative degradation in PPV leads to the appearance of a C=O stretching peak around 1690 cm^{-1}. It is important to note that there is no C=O stretch in the PO-PPV spectra. As

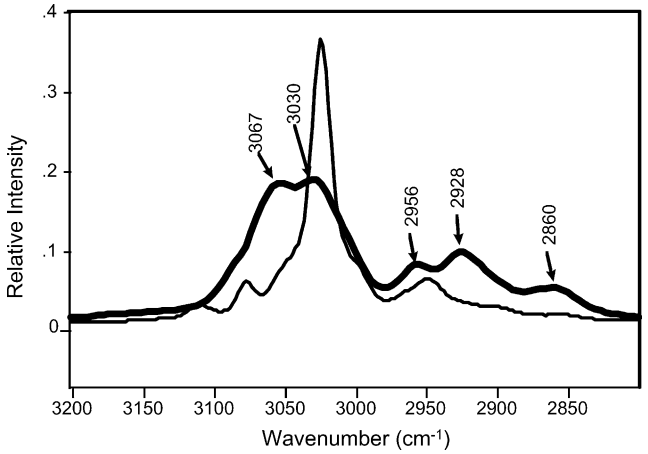

Fig. 8. The infrared absorbance spectra of PO-PPV (thick, peaks labeled) and PPV (thin, no peak labels) in the 3200–2800 cm^{-1} region.

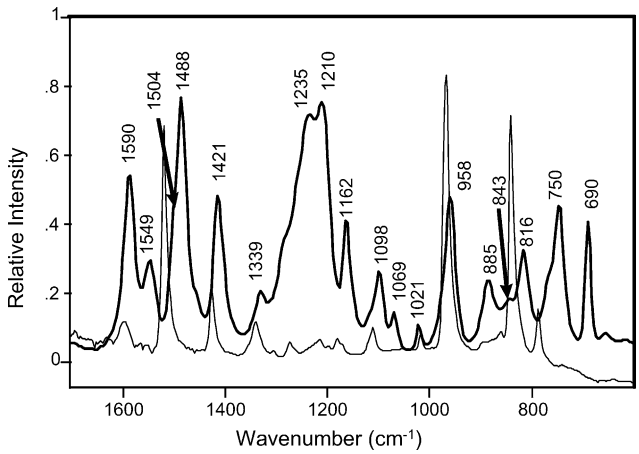

Fig. 9. The infrared absorbance spectra of PO-PPV (thick, peaks labeled) and PPV (thin, no peak labels) in the 1700–600 cm^{-1} region.

expected of a polymer synthesized via the chlorine precursor route, the formation of carbonyl moieties is not a problem during conversion.

As supported by the PPV assignments in Table 2, the majority of vibrational bands within the higher energy half of the fingerprint region (1700–1000 cm^{-1}) are due to aromatic ring stretches and various C–H in-plane bends. The region 1650–1300 cm^{-1} is primarily associated with aromatic ring stretches. The three peaks at 1590, 1488, and 1421 cm^{-1} in the PO-PPV spectra (Fig. 9) can be correlated with the ring stretches at 1594, 1519, and 1424 cm^{-1} observed in PPV. As shown in Table 2, the peaks in PPV correspond with 'quadrant' ring stretch (1594 cm^{-1}) and 'semi-circle' ring stretches (1519 and 1424 cm^{-1}). These specific assignments are not supported in the case of PO-PPV; however, some differentiation between backbone and phenoxy ring stretches has been reported based on the previously mentioned dynamic studies. [10] Based on their dynamic response to a mechanical perturbation, peaks at 1504 and 1421 cm^{-1} have been shown to be associated with the backbone aromatic ring. Similarly, the peak at 1488 cm^{-1} has been shown to be associated with both the backbone and phenoxy substituent. The peak at 1339 cm^{-1} in PO-PPV is present in the PPV spectrum at 1336 cm^{-1} and is identified simply as a ring stretch. The peak at 1549 cm^{-1}, not present in PPV, also falls within this region. Three changes in peak intensity occur in this portion of the spectra during thermal conversion of the PO-PPV precursor to PO-PPV, as seen in Fig. 7b (1625–1510 cm^{-1}). The peak at 1590 cm^{-1} increases slightly. A peak at 1574 cm^{-1} disappears while a peak at lower energy, 1549 cm^{-1}, grows in. A shoulder at 1613 cm^{-1} also disappears. The assignments for all peaks in this region, including those made by dynamic infrared spectroscopy, are supported by the DFT results.

Peaks at 1267, 1176, 1108, and 1013 cm^{-1} in the spectrum of PPV (Table 2) arise from *para*-substituted phenylene C–H in plane deformations. The phenylene C–H in plane deformations in PO-PPV are expected to differ, relative to those in PPV, due to the fact that the ring is 1,2,4-trisubstituted. While PPV lacks any strong vibrations in this region, this is an area of intense absorption for PO-PPV (Fig. 9). Three major peaks at 1235, 1210, and 1162 cm^{-1} are present in the PO-PPV spectra, obscuring the majority of the C-H in-plane deformations. The broad infrared absorbance of these peaks is in the expected region for aryl ether asymmetric and symmetric stretches [29]. The identification of these vibrations as ether stretches is supported by dynamic infrared results as well as DFT calculations. Fig. 7c displays the in situ spectra in the 1300–1175 cm^{-1} region during thermal conversion. The peak at 1250 cm^{-1} can be seen shifting to 1235 cm^{-1}. This indicates that this ether stretch is particularly susceptible to electronic changes along the backbone. The peak at 1210 cm^{-1} exhibits only a small decrease in intensity. A number of peaks in the 1150–1000 cm^{-1} region of PO-PPV (1098, 1069, 1021 cm^{-1}) corresponds with C–H in plane bends.

The lower energy half of the fingerprint region (1000–600 cm^{-1}) of the PO-PPV spectrum is common to C–H and ring out-of-plane bends. Both the PPV and PO-PPV spectra have an intense peak at ~960 cm^{-1}, which has been assigned to *trans*-vinylene C–H out-of-plane bend. As would be expected, this mode increases in intensity during thermal conversion, as seen in Fig. 7d. DFT results for PO-PPV point to a definite *trans*-vinylene C–H out-of-plane bend corresponding with this peak. The only other significant spectral change that occurs in this region is the disappearance of a peak at 920 cm^{-1}. The vibrational mode expected to decrease in intensity is the C–Cl stretch; however, the normal range for this vibration is 850–500 cm^{-1}. Dynamic infrared studies and DFT calculations do not provide any additional information, so the origin of this vibration is left unspecified. If the C–Cl stretch is indeed at lower energy, its intensity is obscured by a number of C–H and ring out-of-plane bends in that region. The PPV spectrum (Fig. 9) exhibits three major peaks at 837, 784, and 556 cm^{-1}, assigned as a *p*-phenylene C–H out of plane bend, origin unknown, and a *p*-phenylene out of plane ring bend, respectively. None of the remaining peaks in this region of the PO-PPV spectrum correspond with any peaks in the spectrum of PPV. Undoubtedly, the 1,2,4-trisubstitution of the backbone ring in PO-PPV results in a unique spectrum in this region. The peaks at 885, 843, and 816 can be labeled as C–H out-of-plane bends. Two strong peaks at 750 and 690 cm^{-1} can confidently be identified as combination C–H and ring out-of-plane deformations arising from the phenoxy substituent. These assignments are strongly supported by the DFT results as well as the dynamic infrared studies. The remaining peaks in this region are likely due to additional C–H and ring out-of-plane bends associated with the backbone of PO-PPV.

4. Conclusions

This study involves the thermal, optoelectronic, mechanical and spectroscopic characterization of PO-PPV and its precursor polymer. It has been seen that PO-PPV has properties comparable to other PPV's, with excellent potential for device applications.

The PO-PPV precursor is easily processible, with good solubility in chloroform and a number of other organic solvents. The excellent quality and mechanical properties (1.7 GPa) of solvent-cast PO-PPV precursor films would be useful in commercial device processing. The glass transition of the precursor occurs near 60 °C, well below the temperature of thermal conversion. As a result, the precursor may be easily molded upon heating without conversion to PO-PPV. In addition, kinetic studies using TGA have shown excellent precursor stability at room temperature. Thermal conversion of the precursor to PO-PPV does not require a reducing atmosphere, and infrared spectroscopy has shown the fully converted PO-PPV to be free of oxidative defects. This is important as these defects act as exciton "quenching" sites, reducing the efficiency of an electroluminescent organic polymer.

Fully converted PO-PPV films appear to be of excellent quality. An increase in elasticity (i.e. rigidity) is seen upon full conversion from the PO-PPV precursor to PO-PPV, undoubtedly due to the induced conjugation. Unprocessed PO-PPV films exhibit a storage modulus above 2 GPa at room temperature, higher than that of unprocessed PPV and polypyrrole. PO-PPV exhibits a glass transition at approximately 125 °C and thermal stability up to 350 °C.

Photoluminescence spectra of PO-PPV indicate light emission at 560 nm in the yellow-green region of the visible spectrum. PO-PPV has been determined by UV–vis spectroscopy to have an approximate bandgap energy of 2.40 eV, within the semi-conducting range. The infrared vibrational spectrum of PO-PPV and its precursor have been characterized. Further studies into potential applications for this PPV derivative are in progress.

Acknowledgements

The authors gratefully acknowledge, Dr. H.R. Kricheldorf for providing a starting material, Dr. Paul Maslen for the DFT calculations, Dr. Jing Li for the use of the X-ray diffractometer and Dr. Long Pan for the X-ray analysis. This material is based upon work supported by the National Science Foundation under Grant Nos. CHE 96-01710 and DMR 00-75820.

References

[1] J.H. Burroughes, D.D.C. Bradley, A.R. Brown, R.N. Marks, K.D. Mackay, R.H. Friend, P.L. Burn, A.B. Holmes, Nature 347 (1990) 539.
[2] A. Kraft, A.C. Grimsdale, A.B. Holmes, Angew. Chem., Int. Ed. 37 (1998) 402.
[3] U. Mitschke, P. Bauerle, J. Mater. Chem. 10 (2000) 1471.
[4] F.R. Denton III, P.M. Lahti, in: D.L. Wise, G.E. Wnek, D.J. Trantolo, T.M. Cooper, J.D. Gresser (Eds.), Photonic Polymer Systems: Fundamentals, Methods and Applications, Marcel Dekker, New York, NY, 1998, p. 61.
[5] B.R. Hsieh, J.C. Salamone, in: J.C. Salamone (Ed.), Polymeric Materials Encyclopedia, vol. 9, CRC Press Inc., Boca Raton, Florida, 1996, 6537.
[6] W.J. Swatos, B. Gordon III, Polym. Prep. 31 (1990) 505.
[7] B.R. Hsieh, W.A. Feld, Polym. Prep. 2 (1993) 410.
[8] B.R. Hsieh, Y. Yu, E.W. Forsythe, G.M. Schaaf, W.A. Feld, J. Am. Chem. Soc. 120 (1998) 231.
[9] W.C. Wan, H. Antoniadis, V.C. Choong, H. Razafitrimo, Y. Gao, W.A. Feld, B.R. Hsieh, B. R. Macromol. 30 (1997) 6567.
[10] J.N. Wilking, C.J. Manning, G.A. Arbuckle-Keil, Appl. Spectrosc. 58 (2004) 304.
[11] H.R. Kricheldorf, V. Doring, V. Eckhardt, Makromol. Chem. 189 (1988) 1425.
[12] J. Kong, C.A. White, A.I. Krylov, D. Sherrill, R.D. Adamson, T.R. Furlani, M.S. Lee, A.M. Lee, S.R. Gwaltney, T.R. Adams, C. Ochsenfeld, A.T.B. Gilbert, G.S. Kedziora, V.A. Rassolov, D.R. Maurice, N. Nair, Y. Shao, N.A. Besley, P.E. Maslen, J.P. Dombroski, H. Daschel, W. Zhang, P.P. Korambath, J. Baker, E.F.C. Byrd, T. Van Voorhis, M. Oumi, S. Hirata, C.-P. Hsu, N. Ishikawa, J. Florian, A. Warshel, B.G. Johnson, P.M.W. Gill, M. Head-Gordon, J.A. Pople, J. Comp. Chem. 21 (2000) 1532.
[13] A.D. Becke, J. Chem. Phys. 98 (1993) 5648.
[14] C. Lee, W. Yang, R.G. Parr, Phys. Rev. B 37 (1988) 785.
[15] H.V. Shah, G.A. Arbuckle, Macromolecules 32 (1999) 5.
[16] H.E. Blair, ASTM STP 1249 (1994) 50.
[17] C.D. Doyle, J. Appl. Polym. Sci. 5 (1961) 285.
[18] J. Wilking, G.A. Arbuckle-Keil, B. Hsieh, The Rutgers Scholar 3 (2001) (http://rutgersscholar.rutgers.edu/volume03/wilkarbu/wilkarbu.htm).
[19] J. Wery, B. Dulieu, M. Baitoul, P. Paniez, G. Froyer, S. Lefrant, Synth. Met. 101 (1999) 194.
[20] O. Schafer, A. Greiner, J. Pommerehne, W. Guss, H. Vestweber, H.Y. Tak, H. Bassler, C. Schmidt, G. Lussem, B. Schartel, V. Stumpflen, J.H. Wendorff, S. Spiegel, C. Moller, H.W. Spiess, Synth. Met. 82 (1996) 1.
[21] Y. Liu, M.S. Liu, X.-C. Li, A.K.-Y. Jen, Chem. Mater. 10 (1998) 3301.
[22] H. Okuzaki, T. Kira, T. Kunugi, J. Appl. Polym. Sci. 75 (2000) 566.
[23] H. Okuzaki, Y. Hirata, T. Kunugi, Polymer 40 (1999) 2625.
[24] T. Kunugi, H. Okuzaki, J. Polym. Sci.: Part B 34 (1996) 1269.
[25] S. Son, A. Dodabalapur, A.J. Lovinger, M.E. Galvin, Science 269 (1995) 376.
[26] R.A. Wessling, R.G. Zimmerman, US Patent 3,401,152 (1968).
[27] L.J. Rothberg, M. Yan, F. Papadimitrakopoulos, M.E. Galvin, E.W. Kwock, T.M. Miller, Synth. Met. 80 (1996) 41.
[28] D.D.C. Bradley, J. Phys. D: Appl. Phys. 20 (1987) 1389.
[29] G. Socrates, Infrared Characteristic Group Frequencies, 2nd ed., Wiley, West Sussex, England, 1994.